

The development and verification of Mixed Potential Integral Equation Field Solvers in Electromagnetics

J. Rodgers and K. Chuang
California State University, Long Beach

Abstract – We provide the theory behind the Method-Of-Moments (MoM) based technique for solving mixed potential electromagnetic integral equations in multilayered media. The dyadic and scalar Green functions for these (MoM) integral equations are derived in the spectral domain in terms of the Transverse Electric (TE) and Transverse Magnetic (TM) transmission line equations. We then discuss how the Generalized Pencil Of Functions (GPOF) method is used to transform these spectral Green functions back to the spatial domain for use in the MoM process. Finally we provide a detailed discussion concerning the verification process with the use of the open source software GLMoM and the Samtec Golden Standard reference structure.

I. Introduction

Electromagnetic field solvers are specialized programs that solve Maxwell's equations directly. Integral equation type field solvers offer the capability to probe inside a multilayered structure to obtain surface currents on metallic conductors buried within the structure (such as the copper traces in printed circuit board assemblies). Once the current distribution throughout a structure is known, both the radiation and propagation of the electromagnetic fields can be investigated.

Verifying the accuracy of electromagnetic field solvers in a quantitative fashion can be difficult, [2]. To do so requires that a well characterized and understood standard be defined, such as that provided by Samtec through the Golden Standard reference structure. The Golden Standard provides a well characterized physical reference for electromagnetic simulation together with a verification methodology in the form of key markers that quantify successful simulation.

In this paper we will use the Samtec Golden Standard reference structure to verify the accuracy of the open source electromagnetic software GLMoM. To accomplish this task we will begin by developing the theory behind Method-of-Moments based integral equation field solvers (such as GLMoM) from first principles. We will then apply this theory directly to the Samtec reference structure to obtain closed form scalar and dyadic Green functions to be used in the MoM integral equations. In this way we hope to elucidate the scope of exactly what is being validated within the electromagnetic software.

Outline of paper:

The first seven sections of this paper give a brief yet concise development of the theory. (The references cited at the end of the paper can be examined for further investigation.) The final and longest section provides the experimental verification which utilizes GLMoM and the Samtec Golden Standard reference structure. Within each of the first theoretical sections we will highlight the pertinent equations developed. If desired, on first reading one can simply skim through these sections taking note of the highlighted equations. Further details can be sought when these equations are referenced in the final experimental section.

In **section I** (this section) we give an introduction and outline of the paper.

In **section II** we derive the Mixed Potential Integral Equation (MPIE) and show how it is used in the Method-Of-Moments (MoM) process to find the surface currents on metallic conductors embedded in planar media. In this early section we will see immediately that the effectiveness of the entire MPIE-MoM process rests on the ability to obtain reliable dyadic and scalar Green functions in a computationally effective way.

In **section III** we derive the Transverse Electric (TE) and Transverse Magnetic (TM) transmission line equations (and corresponding wave equations), starting directly from Maxwell's equations. (In this paper, for the purpose of added clarity over generality, we avoid using network variables and work entirely in terms of the electric and magnetic fields. Please see the appendix for a discussion on the common use of network variables.)

In **section IV** we use the TE and TM based wave equations (derived in section III) to define scalar Green functions for the components of the electric and magnetic fields. (The solution for these Green functions are given in section V). We then derive an expression for the dyadic Green function for the vector potential in terms of the scalar TE and TM component electric and magnetic field Green functions.

In **section V** we solve for the TE and TM based electric and magnetic field Green functions by solving the appropriate wave equations under suitable boundary conditions. General solutions are given in terms of the dielectric layer stack permittivities for the printed circuit board assemblies.

In **section VI** we express the scalar potential Green function in terms of the TE and TM based electric field Green functions.

In **section VII**, the final theory section of the paper, we discuss the Generalized-Pencil-Of-Function (GPOF) method and show how it is used to inverse transform the spectral domain Green functions back to the spatial domain for use in the MoM process.

Section VIII provides experimental verification. The Samtec Golden Standard reference structure will be used to validate the electromagnetic simulation software GLMoM.

Summary and References

II. Integral Equations and the Method-of-Moments

Our first step in implementing the Method-of-Moments (MoM) procedure is to derive an Electric Field Integral Equation (EFIE) that relates an applied incident field to the scattered currents it generates. This section will derive a Mixed Potential Integral Equation (MPIE) which enforces boundary conditions on the tangential components of the electric field at the surface of a conductor.

When an incident electric field is applied in the vicinity of an electric conductor, the total electric field can be written as the sum of the impressed and scattered fields,

$$(II-1) \mathbf{E}_t(r) = \mathbf{E}_i(r) + \mathbf{E}_s(r)$$

Applying the boundary condition, $\mathbf{E}_t = 0$, at the surface of the conductor gives,

$$\mathbf{E}_i(r) = -\mathbf{E}_s(r)$$

Using an $e^{-i\omega t}$ time dependence, the scattered field can be written as,

$$(II-2) \mathbf{E}_s(r) = i\omega\mathbf{A} - \nabla\phi$$

Working in the Lorentz gauge, $\phi = \frac{i\omega}{k^2}\nabla\cdot\mathbf{A}$, equation (2) becomes,

$$(II-3) \mathbf{E}_s(r) = i\omega\mathbf{A} - \nabla\phi = i\omega\mathbf{A} - \frac{i\omega}{k^2}\nabla(\nabla\cdot\mathbf{A}) = i\omega(\underline{\underline{\mathbf{I}}} - \frac{1}{k^2}\nabla\nabla)\cdot\mathbf{A}$$

where $\underline{\underline{\mathbf{I}}}$ is the identity dyad and $\nabla\nabla$ is the gradient-of-divergence dyad.

Now the vector potential is expressed in terms of the dyadic Green's function as [3],[4],

$$(II-4) \mathbf{A} = \int \underline{\underline{\mathbf{G}}}^{AJ}(r, r') \cdot \mathbf{J}_s(r') dr'$$

The scattered field can then be represented as an integral equation involving the dyadic Green's function for \mathbf{A} . Substituting (4) into (3) gives,

$$(II-5) \mathbf{E}_s(r) = i\omega \int \underline{\underline{\mathbf{G}}}^{AJ}(r, r') \cdot \mathbf{J}_s(r') dr' - \frac{i\omega}{k^2} \int [\nabla\nabla \cdot \underline{\underline{\mathbf{G}}}^{AJ}(r, r')] \cdot \mathbf{J}_s(r') dr'$$

The gradient operator is now factored out of the second integral and an appropriate integration-by-parts process (or Green's identity) is applied. Specifically, we seek a scalar valued function G_ϕ such that,

$$(II-6) \frac{i\omega}{k^2} \nabla \cdot \underline{\underline{\mathbf{G}}}^{AJ}(r, r') = \frac{1}{i\omega} \nabla' G_\phi(r, r')$$

Using equation (6) and an integration-by-parts in equation (5) gives an integral equation in terms of the vector potential Green function and the unknown current density \mathbf{J}_s ,

$$(II-7) \mathbf{E}_i(r) = -i\omega \int \underline{\underline{\mathbf{G}}}^{AJ}(r, r') \cdot \mathbf{J}_s(r') dr' + \frac{1}{i\omega} \nabla \int G_\phi(r, r') \nabla' \cdot \mathbf{J}_s(r') dr'$$

Note: It should be pointed out that the use of equation (6) followed by an integration-by-parts is technically only valid in a homogeneous media [5],[6]. When conductors are allowed to penetrate the boundary interfaces of a stratified media, a correction term needs to be added to equation (6). For the Samtec reference structure, no such layer crossing conductors exist and equations (6) and (7) remain valid.

The procedure for determining the dyadic and scalar Green's functions $\underline{\underline{\mathbf{G}}}^{AJ}, G_\phi$ for a given structure will be discussed in the next section. Once the dyadic and scalar Green functions are known, integral equation (7) can be solved using the MoM procedure.

In the MoM procedure, the unknown current density \mathbf{J}_s is expressed as a linear combination of basis functions,

$$(II-8) \mathbf{J}_s(r') = \sum_{q=1}^N i_q \mathbf{B}_q(r')$$

where i_q is the coefficient to be determined and $\mathbf{B}_q(r')$ is the basis function. Inserting summation (8) into integral equation (7) gives,

$$(II-9) \mathbf{E}_i(r) = -i\omega \sum_{q=1}^N i_q \int \underline{\underline{\mathbf{G}}}^{AJ}(r, r') \cdot \mathbf{B}_q(r') dr' + \frac{1}{i\omega} \sum_{q=1}^N i_q \nabla \int G_\phi(r, r') \nabla' \cdot \mathbf{B}_q(r') dr'$$

Now taking the inner product of both sides of the above expression against the basis function $\mathbf{B}_p(r)$, $p = 1, \dots, N$, gives,

$$(II-10a) \langle \mathbf{B}_p(r), \mathbf{E}_i(r) \rangle = -i\omega \sum_{q=1}^N i_q \langle \mathbf{B}_p(r), \int \underline{\underline{\mathbf{G}}}^{AJ}(r, r') \cdot \mathbf{B}_q(r') dr' \rangle + \frac{1}{i\omega} \sum_{q=1}^N i_q \langle \mathbf{B}_p(r), \nabla \int G_\phi(r, r') \nabla' \cdot \mathbf{B}_q(r') dr' \rangle$$

This can be written in matrix notation as

$$(II-10b)$$

$$[\mathbf{V}] = [\mathbf{Z}][\mathbf{I}]$$

where the components of these matrices are $v_p = \langle \mathbf{B}_p(r), \mathbf{E}_i(r) \rangle$, i_q and

$$z_{pq} = -i\omega \langle \mathbf{B}_p(r), \int \underline{\underline{\mathbf{G}}}^{AJ}(r, r') \cdot \mathbf{B}_q(r') dr' \rangle + \frac{1}{i\omega} \langle \mathbf{B}_p(r), \nabla \int G_\phi(r, r') \nabla' \cdot \mathbf{B}_q(r') dr' \rangle$$

This matrix equation can be inverted to find the unknown current coefficients i_q . (See Note*)

Implementing the MoM procedure is, mathematically speaking, the process of solving integral equation (10) in matrix form. The effectiveness of this process rests on finding accurate dyadic $\underline{\underline{\mathbf{G}}}^{AJ}(r, r')$ and scalar $G_\phi(r, r')$ Green functions in a computationally efficient way. The form of these Green functions is highly dependent on the particular geometry under investigation. The specific geometry investigated in this paper is that of planar stratified media as found in commercial printed circuit board assemblies.

Note*: The most common basis functions used in the MoM procedure are the standard RWG (Rao-Wilton-Gilsson) basis, ref [7]. Unfortunately when using the RWG basis at very low frequencies, the MoM matrix representation of the EFIE operator becomes ill-conditioned and inaccurate, ref [8]. To circumvent these difficulties, specialized techniques such as the loop tree discretization can be implemented. This is basically a re-ordering of the MoM matrix providing a highly stable solution at low frequencies. This will be pointed out in the experimental section of this paper.

To derive the dyadic $\underline{\underline{\mathbf{G}}}^{AJ}(r, r')$ and scalar $G_\phi(r, r')$ Green functions, transmission line equations are first specified (directly from Maxwell's equations) for the transverse electric (TE) and transverse magnetic (TM) fields. Scalar electric-field and magnetic-field Green functions are then given for these TE and TM components separately. Finally, the dyadic $\underline{\underline{\mathbf{G}}}^{AJ}(r, r')$ and scalar $G_\phi(r, r')$ Green functions are specified in terms of the TE and TM scalar electric-field and magnetic-field Green functions.

III. The transmission line equations for planar media

With a sinusoidal time dependence of, $e^{-i\omega t}$, Maxwell's equations are written,

$$\nabla \times \mathbf{E} = i\omega\mu\mathbf{H}$$

$$\nabla \times \mathbf{H} = -i\omega\varepsilon\mathbf{E} + \mathbf{J}$$

Maxwell's equations can be decoupled into two sets of equations that describe the transverse electric (TE) and transverse magnetic (TM) fields. A straightforward demonstration of this (for the case of a planar layered media) is to work in a rotated coordinate system where for each wave vector $\bar{\mathbf{K}}$, a rotation is made to a rectangular (u,v,z) coordinate system that brings the wave vector into the u-z plane as shown in figure 1.

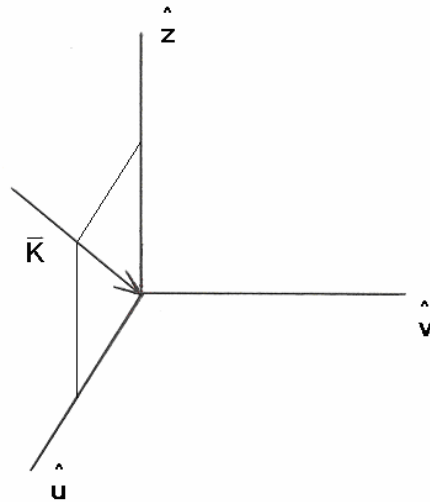


Figure 1. The rotated (u,v,z) coordinate system

In the rotated system, Maxwell's equations can be decoupled by separately considering the two linearly independent sources, $\mathbf{J} = (0, J_v, 0)$ for the TE case, and $\mathbf{J} = (J_u, 0, J_z)$ for the TM case.

Note: By definition, the \hat{u} -coordinate is in the direction of K_ρ (the \mathbf{K} vector projected into the horizontal plane). For this reason we often write K_u and K_ρ interchangeably.

For the TE case, $\mathbf{J} = (0, J_v, 0)$, expanding the curl operators in Maxwell's equations and equating components gives,

$$(III-1) \frac{\partial E_v}{\partial z} = -ik_z Z^h H_u$$

$$(III-2) \frac{\partial H_u}{\partial z} = -ik_z Y^h E_v + J_v$$

$$(III-3) H_z = \frac{k_u}{\omega\mu} E_v$$

For $k_z^2 = \omega^2 \mu\epsilon - k_u^2$, $Z^h = \frac{1}{Y^h} = \frac{\omega\mu}{k_z}$, and corresponding wave equation,

$$(III-5) \frac{\partial^2 E_v}{\partial z^2} + k_z^2 E_v = -ik_z Z^h J_v$$

Likewise for the TM case, $\mathbf{J} = (J_u, 0, J_z)$, Maxwell's equations give,

$$(III-6) \frac{\partial H_v}{\partial z} = ik_z Y^e E_u - J_u$$

$$(III-7) \frac{\partial E_u}{\partial z} = ik_z Z^e H_v + \frac{k_u}{\omega\epsilon} J_z$$

$$(III-8) E_z = -\frac{k_u}{\omega\epsilon} H_v + \frac{1}{i\omega\epsilon} J_z$$

For $k_z^2 = \omega^2 \mu\epsilon - k_u^2$, $Z^e = \frac{1}{Y^e} = \frac{k_z}{\omega\epsilon}$, and corresponding wave equations,

$$(III-9) \frac{\partial^2 E_u}{\partial z^2} + k_z^2 E_u = -ik_z Z^e J_u$$

$$(III-10) \frac{\partial^2 H_v}{\partial z^2} + k_z^2 H_v = ik_z Y^e \left(\frac{k_u}{\omega\epsilon} J_z \right)$$

Equations (III-1) through (III-10) are the transmission line, and wave equations, in the rotated (u,v,z) coordinate system.

IV. The dyadic Green functions

Using wave equations (III-5), (III-9) and (III-10), we can find scalar Green functions for delta current-density sources. This allows us to write,

$$(IV-1) E_u(z) = \int_{-\infty}^{+\infty} E_u^{J_u}(z, z') J_u(z') dz' + \int_{-\infty}^{+\infty} E_u^{J_z}(z, z') \frac{k_u}{\omega \epsilon} J_z(z') dz' = \langle E_u^{J_u}, J_u \rangle + \frac{k_u}{\omega \epsilon} \langle E_u^{J_z}, J_z \rangle$$

$$(IV-2) E_v(z) = \int_{-\infty}^{+\infty} E_v^{J_v}(z, z') J_v(z') dz' = \langle E_v^{J_v}, J_v \rangle$$

$$(IV-3) E_z(z) = \int_{-\infty}^{+\infty} E_z^{J_u}(z, z') J_u(z') dz' + \int_{-\infty}^{+\infty} E_z^{J_z}(z, z') \frac{k_u}{\omega \epsilon} J_z(z') dz' = \langle E_z^{J_u}, J_u \rangle + \langle E_z^{J_z}, \frac{k_u}{\omega \epsilon} J_z \rangle$$

The notation used here, for $E_u^{J_u}$ for example, gives the Green function for the u-component of \mathbf{E} due to a current source $\mathbf{J} = J_u \hat{\mathbf{u}} = \delta(z - z') \hat{\mathbf{u}}$. Note also that $\frac{k_u}{\omega \epsilon}$ has been factored out of the Green functions for the z-component (or alternatively, from equation III-10, the input for the z-component is $\frac{k_u}{\omega \epsilon} J_z$). Note also that using equation (III-8) allows us to write equation (3) as,

$$(IV-4) E_z(z) = \int_{-\infty}^{+\infty} E_z^{J_u}(z, z') J_u(z') dz' + \int_{-\infty}^{+\infty} E_z^{J_z}(z, z') \frac{k_u}{\omega \epsilon} J_z(z') dz' = \langle E_z^{J_u}, J_u \rangle + \langle E_z^{J_z}, \frac{k_u}{\omega \epsilon} J_z \rangle$$

$$= -\frac{k_u}{\omega \epsilon} \langle H_v^{J_u}, J_u \rangle + \frac{1}{i\omega \epsilon} \left\langle \frac{k_u^2}{i\omega \epsilon} H_v^{J_z}(z, z') + \delta(z - z'), J_z \right\rangle$$

Using these components to describe the total electric field gives,

$$E = E_u \hat{\mathbf{u}} + E_v \hat{\mathbf{v}} + E_z \hat{\mathbf{z}} =$$

$$\left(\langle E_u^{J_u}, J_u \rangle + \frac{k_u}{\omega \epsilon} \langle E_u^{J_z}, J_z \rangle \right) \hat{\mathbf{u}} + \langle E_v^{J_v}, J_v \rangle \hat{\mathbf{v}} + \left(-\frac{k_u}{\omega \epsilon} \langle H_v^{J_u}, J_u \rangle + \frac{1}{i\omega \epsilon} \left\langle \frac{k_u^2}{i\omega \epsilon} H_v^{J_z} + \delta(z - z'), J_z \right\rangle \right) \hat{\mathbf{z}}$$

Substituting $J_u = \hat{\mathbf{u}} \cdot \mathbf{J}$, $J_v = \hat{\mathbf{v}} \cdot \mathbf{J}$, and $J_z = \hat{\mathbf{z}} \cdot \mathbf{J}$ gives,

$$\mathbf{E} = \left(\langle E_u^{J_u}, (\hat{\mathbf{u}} \cdot \mathbf{J}) \rangle + \frac{k_u}{\omega \epsilon} \langle E_u^{J_z}, (\hat{\mathbf{z}} \cdot \mathbf{J}) \rangle \right) \hat{\mathbf{u}} + \langle E_v^{J_v}, (\hat{\mathbf{v}} \cdot \mathbf{J}) \rangle \hat{\mathbf{v}} + \left(-\frac{k_u}{\omega \epsilon} \langle H_v^{J_u}, (\hat{\mathbf{u}} \cdot \mathbf{J}) \rangle + \frac{1}{i\omega \epsilon} \left\langle \frac{k_u^2}{i\omega \epsilon} H_v^{J_z} + \delta(z - z'), (\hat{\mathbf{z}} \cdot \mathbf{J}) \right\rangle \right) \hat{\mathbf{z}}$$

This leads us to define the dyadic Green function,

$$(IV-5) \underline{\underline{\mathbf{G}}}^{EJ} = \hat{\mathbf{u}} \hat{\mathbf{u}} E_u^{J_u} + \hat{\mathbf{v}} \hat{\mathbf{v}} E_v^{J_v} - \hat{\mathbf{z}} \hat{\mathbf{u}} \frac{k_u}{\omega \epsilon} H_v^{J_u} + \hat{\mathbf{u}} \hat{\mathbf{z}} \frac{k_u}{\omega \epsilon} E_u^{J_z} + \hat{\mathbf{z}} \hat{\mathbf{z}} \frac{1}{i\omega \epsilon} \left(\frac{k_u^2}{i\omega \epsilon} H_v^{J_z} + \delta(z - z') \right)$$

Similar expressions for the magnetic field can be given as,

$$(IV-6) H_u(z) = \int_{-\infty}^{+\infty} H_u^{J_v}(z, z') J_v(z') dz' = \langle H_u^{J_v}, J_v \rangle$$

(IV-7)

$$H_v(z) = \int_{-\infty}^{+\infty} H_v^{J_u}(z, z') J_u(z') dz' + \int_{-\infty}^{+\infty} E_u^{J_z}(z, z') \frac{k_u}{\omega \epsilon} J_z(z') dz' = \langle H_v^{J_u}, J_u \rangle + \frac{k_u}{\omega \epsilon} \langle H_u^{J_z}, J_z \rangle$$

$$(IV-8) H_z(z) = \int_{-\infty}^{+\infty} H_z^{J_v}(z, z') J_v(z') dz' = \langle H_z^{J_v}, J_v \rangle = \left\langle \frac{k_u}{\omega \mu} E_v^{J_v}, J_v \right\rangle$$

$$H = H_u \hat{u} + H_v \hat{v} + H_z \hat{z} = \langle H_u^{J_v}, J_v \rangle \hat{u} + \left(\langle H_v^{J_u}, J_u \rangle + \frac{k_u}{\omega \epsilon} \langle H_u^{J_z}, J_z \rangle \right) \hat{v} + \frac{k_u}{\omega \mu} \langle E_v^{J_v}, J_v \rangle \hat{z}$$

Again substituting $J_u = \hat{u} \cdot \mathbf{J}$, $J_v = \hat{v} \cdot \mathbf{J}$, and $J_z = \hat{z} \cdot \mathbf{J}$ gives,

$$H = H_u \hat{u} + H_v \hat{v} + H_z \hat{z} = \langle H_u^{J_v}, \hat{v} \cdot \mathbf{J} \rangle \hat{u} + \left(\langle H_v^{J_u}, \hat{u} \cdot \mathbf{J} \rangle + \frac{k_u}{\omega \epsilon} \langle H_u^{J_z}, \hat{z} \cdot \mathbf{J} \rangle \right) \hat{v} + \frac{k_u}{\omega \mu} \langle E_v^{J_v}, \hat{v} \cdot \mathbf{J} \rangle \hat{z}$$

$$(IV-9) \underline{\underline{\mathbf{G}}}^{HJ} = \hat{u} \hat{v} H_u^{J_v} + \hat{v} \hat{u} H_v^{J_u} + \hat{z} \hat{v} \frac{k_u}{\omega \mu} E_v^{J_v} + \hat{v} \hat{z} \frac{k_u}{\omega \epsilon} H_u^{J_z}$$

Equations (IV-5) and (IV-9) give the electric field dyadic Green function and magnetic field dyadic Green function respectively.

To arrive at the vector potential dyadic Green function we substitute,

$$\mathbf{A} = \langle \underline{\underline{\mathbf{G}}}^{AJ}, \mathbf{J} \rangle$$

into the defining relationship for \mathbf{A} ,

$$\mu \mathbf{H} = \nabla \times \mathbf{A}$$

This gives,

$$\mu \mathbf{H} = \mu \langle \underline{\underline{\mathbf{G}}}^{HJ}, \mathbf{J} \rangle = \nabla \times \mathbf{A} = \nabla \times \langle \underline{\underline{\mathbf{G}}}^{AJ}, \mathbf{J} \rangle$$

or,

$$(IV-10) \mu \underline{\underline{\mathbf{G}}}^{HJ} = \nabla \times \underline{\underline{\mathbf{G}}}^{AJ}$$

We then stipulate the following formulation for $\underline{\underline{\mathbf{G}}}^{AJ}$ [5],[6],

$$(IV-11) \underline{\underline{\mathbf{G}}}^{AJ} = G_{vv}^{AJ} \hat{u} \hat{u} + G_{vv}^{AJ} \hat{v} \hat{v} + G_{zu}^{AJ} \hat{z} \hat{u} + G_{zz}^{AJ} \hat{z} \hat{z}$$

Using this formulation, the curl operation is performed on the right side of (IV-10) and equated with the left side as given by equation (IV-9). On equating components and using the transmission line equations from section III to simplify gives,

$$(IV-12) G_{zz}^{AJ} = -\frac{\mu}{i\omega\epsilon} H_v^{J_z}$$

$$(IV-13) G_{vv}^{AJ} = \frac{1}{i\omega} E_v^{J_v}$$

$$(IV-14) G_{zu}^{AJ} = -\frac{\mu}{ik_u} (H_u^{J_v} + H_v^{J_u})$$

In matrix notation equations (IV-12)-(IV-14) give,

$$(IV-15) \underline{\underline{\mathbf{G}}}^{AJ} = \begin{pmatrix} G_{uu}^{AJ} & 0 & 0 \\ 0 & G_{vv}^{AJ} & 0 \\ G_{zu}^{AJ} & 0 & G_{zz}^{AJ} \end{pmatrix} = \begin{pmatrix} \frac{1}{i\omega} E_v^{J_v} & 0 & 0 \\ 0 & \frac{1}{i\omega} E_v^{J_v} & 0 \\ -\frac{\mu}{ik_u} (H_u^{J_v} + H_v^{J_u}) & 0 & -\frac{\mu}{i\omega\epsilon} H_v^{J_z} \end{pmatrix}$$

Equation (IV-15) gives the vector potential dyadic Green function in terms of the (TE and TM) scalar electric and magnetic field Green functions. The scalar electric and magnetic field Green functions are found by solving the wave equations (III-5), (III-9), and (III-10) under suitable boundary conditions as discussed in the next section.

V. Derivation of the scalar electric and magnetic field Green functions

In this section the scalar Green functions will be given for the TE and TM components of the electric and magnetic field. To find the TE Green function for the electric field we solve the corresponding wave equation (III-5), rewritten here as,

$$(V-1) \frac{\partial^2 E_v}{\partial z^2} + k_z^2 E_v = -ik_z Z^h \delta(z - z')$$

with $k_z^2 = \omega^2 \mu \epsilon - k_u^2$, $Z^h = \frac{1}{Y^h} = \frac{\omega \mu}{k_z}$, and boundary conditions specified according to the given dielectric layer stack as shown in figure 2.

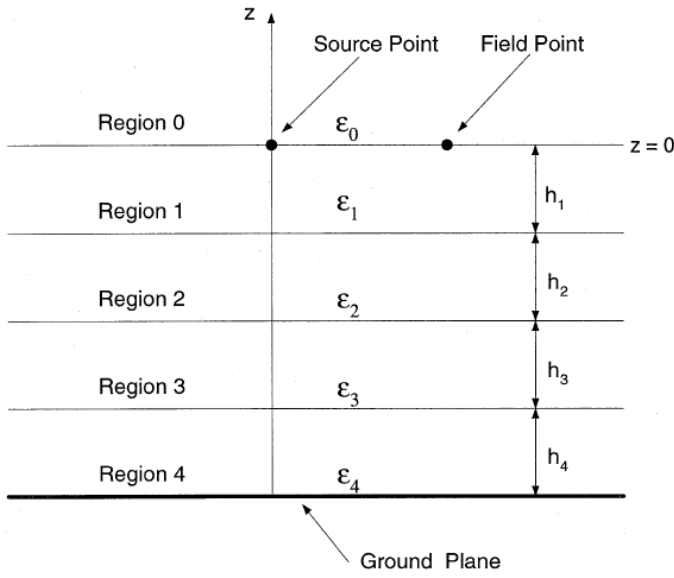


Figure 2. Transmission line representation for layered media

The free space (or single-layer) solution to (1) in an infinite media is given by [9],

$$(V-2) E_v^J(z, z') = \frac{Z^h}{2} e^{-ik_z |z - z'|}$$

Equation (2) can be used to find the multilayered solution by adding homogeneous solutions to (1) so that the boundary conditions at the dielectric interfaces are satisfied. Following this approach, the electric field in layer n is written as[3],

$$(V-3) E_v^J(z | z'; k_{zn}) = \frac{Z_n^h}{2} [e^{-ik_{zn} |z - z'|} + A_n e^{ik_{zn} z} + B_n e^{-ik_{zn} z}]$$

(where the subscript on k_{zn} and Z_n^h indicate the quantity in layer n). The last two terms are due to the reflected waves at the boundaries at $z = z_{n+1}$ and $z = z_n$. The downward going wave for $z > z'$ is a consequence of the reflection of the upward going wave for $z > z'$ at $z = z_n$. Mathematically this relation can be expressed as,

$$A_n e^{ik_{zn}z_n} = \bar{\Gamma}_n^h [e^{-ik_{zn}(z_n-z')} + B_n e^{-ik_{zn}z_n}]$$

$$B_n e^{-ik_{zn}z_{n+1}} = \bar{\Gamma}_n^h [e^{-ik_{zn}(z'-z_{n+1})} + A_n e^{ik_{zn}z_{n+1}}]$$

Where the generalized reflection coefficients, looking up and down respectively, are given by,

$$(V-4) \bar{\Gamma}_n^h \equiv \frac{\bar{Z}_n - Z_n}{\bar{Z}_n + Z_n}$$

$$(V-5) \bar{\Gamma}_n^h \equiv \frac{\bar{Z}_n - Z_n}{\bar{Z}_n + Z_n}$$

and the wave impedances looking up and down are given by,

$$(V-6) \bar{Z}_n = Z_{n-1} \left(\frac{\bar{Z}_{n-1} + iZ_{n-1}t_{n-1}}{Z_{n-1} + i\bar{Z}_{n-1}t_{n-1}} \right)$$

$$(V-7) \bar{Z}_n = Z_{n+1} \left(\frac{\bar{Z}_{n+1} + iZ_{n+1}t_{n+1}}{Z_{n+1} + i\bar{Z}_{n+1}t_{n+1}} \right)$$

with $Z_n = Z_n^h = \omega\mu_n / k_{zn}$ for TE waves. Finally $t_n = \tan(k_{zn}d_n)$, $d_n = z_n - z_{n+1}$.

Now solving for A_n and B_n and substituting back into (V-3) gives,

$$(V-8) E_v^J(z | z'; k_{zn}) = \frac{Z_n^h}{2} (e^{-ik_{zn}|z-z'|} + \frac{1}{D_n^p} [\bar{\Gamma}_n^h e^{-ik_{zn}((z+z')-2z_{n+1})} + \bar{\Gamma}_n^h e^{-ik_{zn}(2z_n-(z+z'))} + \bar{\Gamma}_n^h \bar{\Gamma}_n^h e^{-ik_{zn}(2(z_n-z_{n+1})-(z-z'))} + \bar{\Gamma}_n^h \bar{\Gamma}_n^h e^{-ik_{zn}(2(z_n-z_{n+1})+(z-z'))}]])$$

Equation (V-8) is the scalar electric field Green function for multilayered media. Using transmission line equation, $H_u^J = \frac{1}{-ik_z Z^h} \frac{\partial E_v^J}{\partial z}$, gives on differentiating equation (V-8),

$$(V-9) H_u^J(z | z'; k_{zn}) = \frac{1}{2} (\pm e^{-ik_{zn}|z-z'|} - \frac{1}{D_n^h} [-\bar{\Gamma}_n^h e^{-ik_{zn}((z+z')-2z_{n+1})} + \bar{\Gamma}_n^h e^{-ik_{zn}(2z_n-(z+z'))} - \bar{\Gamma}_n^h \bar{\Gamma}_n^h e^{-ik_{zn}(2(z_n-z_{n+1})-(z-z'))} + \bar{\Gamma}_n^h \bar{\Gamma}_n^h e^{-ik_{zn}(2(z_n-z_{n+1})+(z-z'))}]])$$

Where the upper and lower signs pertain to $z > z'$ and $z < z'$ respectively.

The wave equation for the TM component of the electric field is (III-9),

$$\frac{\partial^2 E_u}{\partial z^2} + k_z^2 E_u = -ik_z Z^e J_u$$

with $k_z^2 = \omega^2 \mu \epsilon - k_u^2$ and $Z^e = \frac{1}{Y^e} = \frac{k_z}{\omega \epsilon}$. It follows that an identical solution is given by,

$$(V-10) E_u^J(z | z'; k_{zn}) = \frac{Z_n^e}{2} (e^{-ik_{zn}|z-z'|} + \frac{1}{D_n^e} [\bar{\Gamma}_n^e e^{-ik_{zn}((z+z')-2z_{n+1})} + \bar{\Gamma}_n^e e^{-ik_{zn}(2z_n-(z+z'))} + \bar{\Gamma}_n^e \bar{\Gamma}_n^e e^{-ik_{zn}(2(z_n-z_{n+1})-(z-z'))} + \bar{\Gamma}_n^e \bar{\Gamma}_n^e e^{-ik_{zn}(2(z_n-z_{n+1})+(z-z'))}]])$$

where we simply replace the wave impedance $Z_n^h = \omega\mu_n / k_{zn}$ with $Z_n^e = \frac{k_{zn}}{\omega\varepsilon_n}$ in all

expressions. Now using transmission line equation, $H_v^{J_u} = \frac{1}{ik_z Z^e} \frac{\partial E_u^{J_u}}{\partial z}$, gives on

differentiating equation (V-10),

$$(V-11) \quad H_v^{J_u}(z | z'; k_{zn}) = \frac{1}{2} (\pm e^{-ik_{zn}|z-z'|} + \frac{1}{D_n^e} [-\bar{\Gamma}_n^e e^{-ik_{zn}((z+z')-2z_{n+1})} + \bar{\Gamma}_n^e e^{-ik_{zn}(2z_n-(z+z'))} - \bar{\Gamma}_n^e \bar{\Gamma}_n^e e^{-ik_{zn}(2(z_n-z_{n+1})-(z-z'))} + \bar{\Gamma}_n^e \bar{\Gamma}_n^e e^{-ik_{zn}(2(z_n-z_{n+1})+(z-z'))}]])$$

Finally the wave equation (III-10) for the TM component of the magnetic field is,

$$\frac{\partial^2 H_v}{\partial z^2} + k_z^2 H_v = ik_z Y^e \left(\frac{k_u}{\omega\varepsilon} J_z \right)$$

with $k_z^2 = \omega^2 \mu\varepsilon - k_u^2$ and $Z^e = \frac{1}{Y^e} = \frac{k_z}{\omega\varepsilon}$ as above. Due to the similar form of equation

(V-8), it follows that the same solution can be used here with the wave admittance Y^e replacing the wave impedance in (V-8). Hence,

$$(V-12) \quad H_v^{J_z}(z | z'; k_{zn}) = \frac{Y_n^e}{2} (e^{-ik_{zn}|z-z'|} + \frac{1}{D_n^e} [\bar{\Gamma}_n^e e^{-ik_{zn}((z+z')-2z_{n+1})} + \bar{\Gamma}_n^e e^{-ik_{zn}(2z_n-(z+z'))} + \bar{\Gamma}_n^e \bar{\Gamma}_n^e e^{-ik_{zn}(2(z_n-z_{n+1})-(z-z'))} + \bar{\Gamma}_n^e \bar{\Gamma}_n^e e^{-ik_{zn}(2(z_n-z_{n+1})+(z-z'))}]])$$

where again we have replaced the wave impedance $Z_n^e = \frac{k_{zn}}{\omega\varepsilon_n}$ with $Y_n^e = \frac{1}{Z_n^e}$ in all expressions.

Equations (V-8) through (V-12) give the scalar components of the electric and magnetic Green functions which are necessary to compute the vector potential dyadic Green function $\underline{\underline{\mathbf{G}}}^{AJ}$ given in equation (IV-15). In the next section it will be shown how the scalar potential Green G_ϕ is also written in terms of equations (V-8) through (V-12).

VI. The scalar potential Green function

Recall that in section I, the following identity was used in deriving the Electric field integral equation,

$$(VI-1) \frac{i\omega}{k^2} \nabla \cdot \underline{\underline{\mathbf{G}}}^{AJ}(\mathbf{r}, \mathbf{r}') = \frac{1}{i\omega} \nabla' G_\phi(\mathbf{r}, \mathbf{r}')$$

As previously mentioned, when conducting surfaces are present that penetrate the dielectric layers, equation (1) needs to be modified by adding a correction term of the form [5],[6],

$$(VI-2) \frac{i\omega}{k^2} \nabla \cdot \underline{\underline{\mathbf{G}}}^{AJ}(\bar{\mathbf{r}} | \bar{\mathbf{r}}') = \frac{1}{i\omega} \nabla' K_\phi(\bar{\mathbf{r}} | \bar{\mathbf{r}}') + i\omega C_\phi \hat{\mathbf{z}}$$

Where $\underline{\underline{\mathbf{G}}}^{AJ}$ is the Green function in the n-th layer due to a point current density which is also in the n-th layer. In the case where there are no z-directed conductors penetrating the layers, equation (2) will reduce to equation (1). To find K_ϕ and C_ϕ , we work in the spectral domain with the standard formulation of $\underline{\underline{G}}^A$ used previously,

$\underline{\underline{\mathbf{G}}}^{AJ} = G_{vv}^{AJ} \hat{\mathbf{u}} \hat{\mathbf{u}} + G_{vv}^{AJ} \hat{\mathbf{v}} \hat{\mathbf{v}} + G_{zu}^{AJ} \hat{\mathbf{z}} \hat{\mathbf{u}} + G_{zz}^{AJ} \hat{\mathbf{z}} \hat{\mathbf{z}}$. Substituting this formulation into equation (VI-2) and using the transmission line equations (while noting that in the primed coordinates $\nabla' = -ik_u \hat{\mathbf{u}} + \hat{\mathbf{z}} \frac{d}{dz}$) gives:

$$(4) K_\phi = \frac{-i\omega}{k_u^2} (E_v^{J_v} - E_u^{J_u})$$

Similarly, from,

$$C_\phi = \frac{1}{i\omega\epsilon} \frac{d}{dz} H_v^{J_z} + \frac{d}{dz} K_\phi^n$$

We have,

$$(VI-5) C_\phi = \frac{i\omega}{k_u^2} E_u^{J_z}$$

Note that if there are no z-directed conductors (as in the Samtec reference structure) then $J_z = 0$ and hence the correction factor $C_\phi = 0$. In this case K_ϕ reduces to the typical scalar potential G_ϕ from equation (VI-1) giving,

$$(VI-6) G_\phi = K_\phi = \frac{-i\omega}{k_u^2} (E_v^{J_v} - E_u^{J_u})$$

Equations (IV-15) and (VI-6) give $\underline{\underline{\mathbf{G}}}^{AJ}$ and G_ϕ in the spectral domain. To use these Green functions in the MoM procedure they need to be inverse Fourier transformed back to the spatial domain as discussed in the next section.

VII. Inverse transforming to the spatial domain

Once the Green functions are known in the spectral domain, they can be transformed back to the spatial domain by way of an Inverse Fourier transform. As a specific example, the uu component of the Dyadic Green function for the vector magnetic potential is given as (see *Note below):

$$(VII-1) \quad G_{uu}^A(\bar{\rho}, z | z') = \mathfrak{F}^{-1} \tilde{G}_{uu}^A(\bar{k}_\rho; z | z') = \frac{1}{(2\pi)^2} \int_{-\infty}^{+\infty} \int_{-\infty}^{+\infty} \tilde{G}_{uu}^A(\bar{k}_\rho; z | z') e^{-ik_x x - ik_y y} dk_x dk_y$$

Changing variables to,

$$k_x = k_\rho \cos k_\phi \quad x = \rho \cos \phi$$

$$k_y = k_\rho \sin k_\phi \quad y = \rho \sin \phi$$

allows equation (VII-1) to be written as [3],

$$(VII-2) \quad G_{uu}^A(\bar{\rho}, z | z') = \frac{1}{4\pi} \int_{-\infty}^{+\infty} k_\rho H_0^{(2)}(k_\rho \rho) \tilde{G}_{uu}^A(k_\rho; z | z') dk_\rho$$

where $H_0^{(2)}$ is the zeroth order Hankel function of the second kind.

Although the integrations above are indicated to be along the real axis (as shown by path C_0 in figure 3), the variable k_ρ is in general complex. From Cauchy's theorem we can deform the path of integration (along any path where the argument of the integral remains analytic) without changing the value of the integral [10]. This is shown as path C_1 in the figure where the branch cut of $H_0^{(2)}$ and the poles of \tilde{G}_{uu}^A have been avoided.

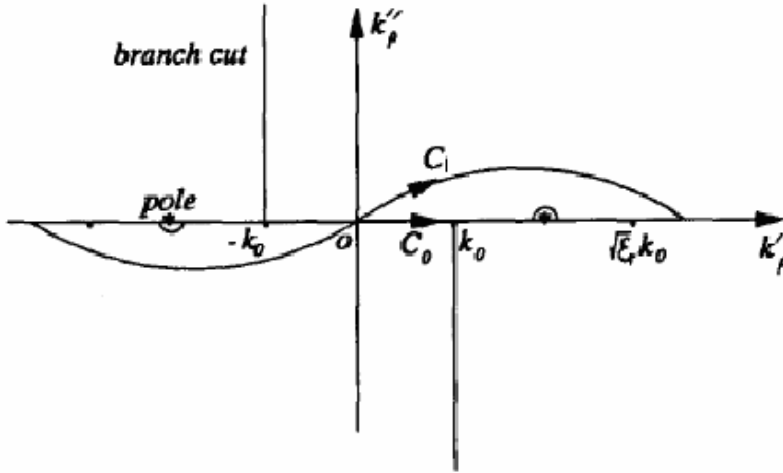


Figure 3. The integration contours C_0 and C_1 on the k_ρ plane

* Note: In this and the remaining sections we are using an e^{+iot} time dependence to be consistent with the software GLMoM. The use of an e^{-iot} time dependence simply requires using the zeroth order Hankel function of the first kind $H_0^{(1)}$ with an inverted contour.

Now in each layer n , we have $k_{zn}^2 = k_n^2 - k_\rho^2$ where $k_n = \omega\sqrt{\mu_n\epsilon_n}$. Transforming the integration contours C_0 and C_1 to the k_z plane gives the contours shown in Figure 4.

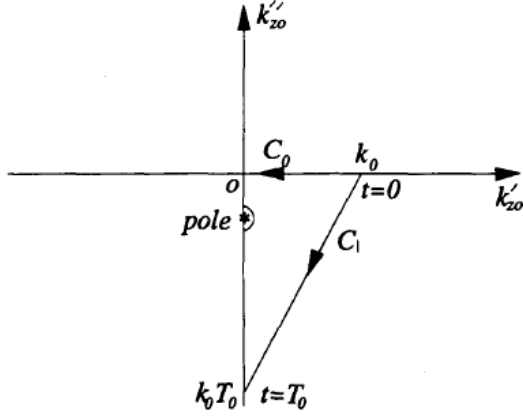


Figure 4. The integration contours C_0 and C_1 on the k_z plane

If the spectral-domain Green's function \tilde{G}_{uu}^A can be approximated by exponentials, then integral (2) can be evaluated analytically using the well-known Sommerfeld identity [3],

$$(VII-3) \frac{e^{-ikr}}{r} = \int_{SIP} dk_\rho k_\rho H_0^{(2)}(k_\rho \rho) \frac{e^{-ik_z|z|}}{2ik_z}.$$

Note that the exponentials in the Sommerfeld identity are given in terms of k_z , not k_ρ , which explains the desire to specify the deformed path C_1 as transformed to the k_z plane.

The finite path C_1 shown in Figure 4 is defined parametrically by,

$$(VII-4) k_z = k[-it + (1 - \frac{t}{T_0})], \quad 0 \leq t \leq T_0$$

where k_z and k are defined in the source layer [10],[11].

The Green functions are sampled uniformly on $t \in [0, T_0]$, which maps onto the path C_1 via equation (VII-4), where they can easily be put in the form of exponentials of k_z . This scheme is called a one-level approximation approach because the complex function to be approximated is sampled between zero and T_0 and is assumed to be negligible beyond T_0 . In cases where the Green functions are highly oscillatory and decay slowly, the uniform sampling and truncation can be problematic. In these cases the one-level approach described here can be extended to a two-level approach as described in the literature [10],[11].

The exponential approximation is typically performed using the generalized pencil-of-functions (GPOF) method as described in [12]. Given the sampled values of the Green function along the path described by equation (4), the GPOF routine will return constants

a_m and b_m such that,

$$(VII-5) i2k_{zn} \tilde{G}^A \simeq \sum_{m=1}^N a_m e^{-b_m k_{zn}}$$

It follows that,

$$(VII-6) \tilde{G}^A \simeq \sum_{m=1}^N a_m \frac{e^{-b_m k_{zn}}}{i2k_{zn}}$$

The Sommerfeld identity (3) can then be used on each exponential term resulting in the spatial-domain expression,

$$(VII-7) G^A \simeq \frac{1}{4\pi} \sum_{m=1}^N a_m \frac{e^{-ib_m k_{zn} r_m}}{r_m}$$

where $r_m = \sqrt{\rho^2 + (z - z' - ib_m)^2}$.

VIII. Experimental Verification

Introduction

In this section, the theory described above will be validated by comparing an open source software program that implements these equations against a known “Device Under Test” (DUT). Specifically, the open source electrical simulation software GLMoM will be used in conjunction with the Samtec Golden Standard Reference Structure.

GLMoM is a Method of Moments based software program written by Yaxun Liu. It has a graphical component based on OpenGL that allows a user to draw the conductor traces of an arbitrary printed circuit board layout (via a script language).

The Samtec Golden Standard reference structure was specifically designed to validate and debug electrical simulation software. The Golden Standard reference board is shown in figure 5. A complete description of this board is documented in [14].



Figure 5. Samtec Reference Structure

From figure 5 it is seen immediately that the Golden Standard reference board is constructed in the fashion of a classical microstrip directional coupler. Figure 6 shows the layer stack-up for this board, along with the copper trace dimensions.

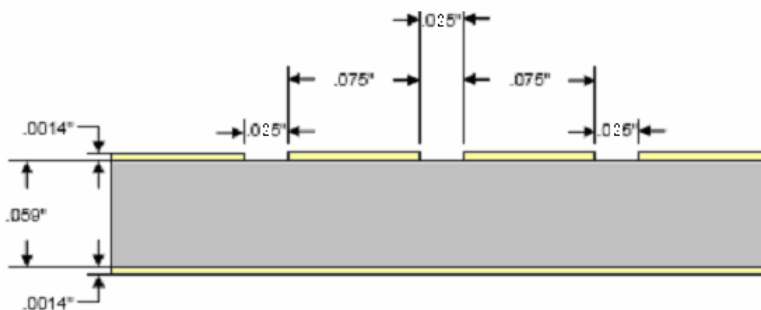


Figure 6. Samtec Reference Board dimensions

Limitations

The Samtec reference structure is a two-dimensional structure. The copper traces are located only on the top horizontal x-y plane (alternatively on the rotated u-v plane). Thus the z-component of the electric field will not enter into the Method-of-Moments matrix calculation. To see this directly note that the unknown current density is written in terms of the basis functions as,

$$(VIII-1) \mathbf{J}_s(r') = \sum_{q=1}^N i_q \mathbf{B}_q(r')$$

The basis functions \mathbf{B}_q (and the scattered current density they approximate) are vectors in the horizontal plane. When they are used to determine the MoM matrix elements, as in, (VIII-2)

$$\langle \mathbf{B}_p(r), \mathbf{E}_i(r) \rangle = -i\omega \sum_{q=1}^N i_q \langle \mathbf{B}_p(r), \int \underline{\underline{\mathbf{G}}}^{AJ}(r, r') \cdot \mathbf{B}_q(r') dr' \rangle + \frac{1}{i\omega} \sum_{q=1}^N i_q \langle \mathbf{B}_p(r), \nabla \int G_\phi(r, r') \nabla' \cdot \mathbf{B}_q(r') dr' \rangle$$

it is seen that they will annihilate the z-component of the electric field (i.e. will project it to zero). For this reason when field solvers such as GLMoM analyze two-dimensional structures they need only evaluate the following components of the dyadic and scalar Green functions respectively,

$$(VIII-3) G_{uu}^{AJ} = G_{vv}^{AJ} = \frac{1}{i\omega} E_v^{J_v} \quad (VIII-4) G_\phi = \frac{-i\omega}{k_u^2} (E_v^{J_v} - E_u^{J_u})$$

Thus the remaining components of the magnetic potential dyad are not directly verified.

Layer Stack Description

As shown in figure 6, the Samtec reference board is a single layer FR4 board with a copper-clad ground plane. The FR4 board, together with the air above it, make up a two layered structure. The Layer Setup window for GLMoM is shown in Figure 7.

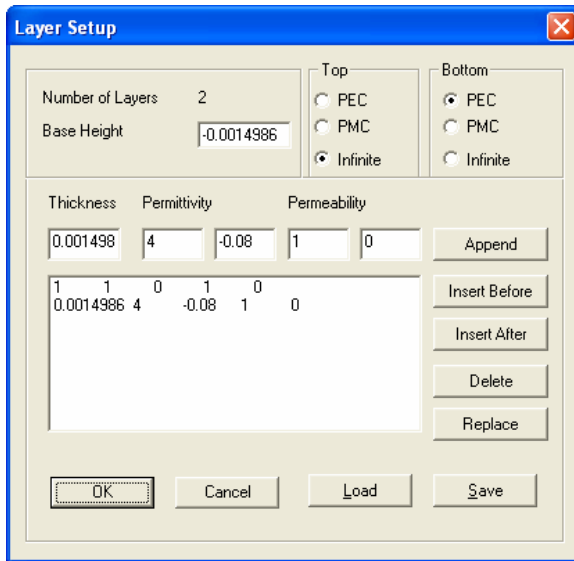


Figure 7. GLMoM Layer Setup dialog box

The thickness of the substrate (FR4 board) is 59 mils (or .0014986 m). In this setup, the air-substrate interface is set to lie in the $z=0$ plane. The base of the assembly (the copper ground plane) is at $z=-0.0014986$ and the **PEC** (Perfect Electric Conductor) radio button is selected in the *Bottom* group box to indicate this ground plane. The **Infinite** radio button is selected in the *Top* group box to indicate that the top air layer, with an arbitrarily selected thickness of 1 meter, actually extends to infinity (this is accomplished internally by setting the reflection-coefficient-looking-up to zero). The FR4 substrate material is modeled with a complex permittivity,

$$\varepsilon = \varepsilon' - i\varepsilon'' = \varepsilon' - i\varepsilon' \tan \delta = \varepsilon' (1 - i \tan \delta) = \varepsilon_r \varepsilon_0 (1 - i \tan \delta)$$

In Figure 7, the (real) relative permittivity is $\varepsilon_r = 4.0$ and the loss tangent is $\tan \delta = 0.02$ (These are the model parameter values sited in the Samtec documentation).

Calculation of the scalar Green functions

The first step in the numerical process is to calculate the scalar Green functions $E_v^{J_v}$, $H_u^{J_u}$, $E_u^{J_u}$, $H_v^{J_v}$, from the given layer parameters. These are given by equations (V-8) through (V-12).

As an example, consider calculating the Green Functions $E_v^{J_v}$ and $E_u^{J_u}$ at a frequency of 1GHz (and along the k_ρ integration path as discussed in section VII). For a given frequency f and k_ρ value, the following parameters are calculated for each layer n:

$$k_n = \omega \sqrt{\mu_n \varepsilon_n} = 2\pi f \sqrt{\mu_n \varepsilon_n} = 2\pi f \sqrt{\mu_0 \varepsilon_0 \varepsilon_{r_n}} = \frac{2\pi f}{c} \sqrt{\varepsilon_{r_n}}$$

$$\gamma_n = \sqrt{k_\rho^2 - k_n^2}$$

$$k_{zn} = \sqrt{k_n^2 - k_\rho^2} = \frac{\gamma_n}{i}$$

$t_n = \tan(k_{zn} d_n)$, where $d_n = z_n - z_{n+1}$ is the thickness of layer n.

And finally, the wave impedance of each layer,

$$Z_n^h = \omega \mu_0 / k_{zn} \text{ for TE waves and } Z_n^e = \frac{k_{zn}}{\omega \varepsilon_n} \text{ for TM waves}$$

These parameters are then used to calculate the generalized wave impedances and the generalized reflection coefficients (looking up and looking down). From section V we have the generalized reflection coefficients looking up and down (where p is either e for TM waves or h for TE waves),

$$(VIII-5) \bar{\Gamma}_n^p \equiv \frac{\bar{Z}_n^p - Z_n^p}{\bar{Z}_n^p + Z_n^p}$$

$$(VIII-6) \bar{\Gamma}_n^p \equiv \frac{\bar{Z}_n^p - Z_n^p}{\bar{Z}_n^p + Z_n^p}$$

and the generalized wave impedances looking up and down,

$$(VIII-7) \bar{Z}_n^p = Z_{n-1}^p \left(\frac{\bar{Z}_{n-1}^p + iZ_{n-1}^p t_{n-1}}{Z_{n-1}^p + i\bar{Z}_{n-1}^p t_{n-1}} \right)$$

$$(VIII-8) \bar{Z}_n^p = Z_{n+1}^p \left(\frac{\bar{Z}_{n+1}^p + iZ_{n+1}^p t_{n+1}}{Z_{n+1}^p + i\bar{Z}_{n+1}^p t_{n+1}} \right)$$

Here $n=0$ for layer 0, which is the air layer, and $n=1$ for the substrate layer.

On calculating these generalized values (and dropping the superscript p), the following facts are noticed:

Generalized Wave Impedance in Layer 0 (the air layer)

A. The generalized wave impedance looking up from layer 0 is just $\bar{Z}_0 = Z_0$, the wave impedance of layer 0. This is true because the air medium extends to infinity by the selection of the **Infinite** button in the *Top* group box. This means that there is no reflected “down-going” wave from this medium.

B. The generalized wave impedance looking down from layer 0 is $\bar{Z}_0 = iZ_1 \tan(k_{z1}d_1)$. This formula is recognized as the standard formula for a transmission line of length d_1 which is shorted at the load. In this case the transmission line is the substrate (of thickness d_1) and the short is the ground plane.

Generalized Wave Impedance in Layer 1 (the substrate layer)

A. The generalized wave impedance looking up from layer 1 is again $\bar{Z}_1 = Z_0$, the wave impedance of layer 0. This is true for the same reason given above; there is no reflected “down-going” wave from layer 0 (the air layer).

B. The generalized wave impedance looking down from layer 1 is $\bar{Z}_1 = 0$. This is due to the ground plane and is a result of the selection of the PEC button in the *Bottom* group box.

Once the generalized wave impedances have been calculated, the generalized reflection coefficients can be found.

Generalized Reflection Coefficient in Layer 0 (the air layer)

A. The generalized reflection coefficient looking up from layer 0 is $\bar{\Gamma}_0 = 0$. Again this is true since there is no reflected “down-going” wave from layer 0 (the air layer).

B. The generalized reflection coefficient looking down from layer 0 is,

$$\bar{\Gamma}_0 = \frac{iZ_1 \tan(k_{z1}d_1) - Z_0}{iZ_1 \tan(k_{z1}d_1) + Z_0}$$

This formula is again recognized as the standard formula for a transmission line of impedance Z_0 (the wave impedance of air) looking into a load with impedance $iZ_1 \tan(k_{z_1}d_1)$ (the wave impedance of the substrate with a ground plane).

Generalized Reflection Coefficient in Layer 1 (the substrate layer)

A. The generalized reflection coefficient looking up from layer 1 is,

$$\bar{\Gamma}_1 = \frac{Z_0 - Z_1}{Z_0 + Z_1}$$

Again due to the infinite extent of layer 0, the generalized reflection coefficient from layer 1 looking into layer 0 reduces to the standard Fresnel reflection coefficient as expected.

B. The generalized reflection coefficient looking down from layer 1 is $\bar{\Gamma}_1 = -1$. This is the expected result due to the PEC ground plane.

Now that we have the upward looking and downward looking generalized reflection coefficients for each layer, we can calculate the Green functions $E_v^{J_v}$ and $E_u^{J_u}$. From equation (V-8),

$$(VIII-9) \quad E_v^{J_v}(z | z'; k_{z_n}) = \frac{Z_n^h}{2} (e^{-ik_{z_n}|z-z'|} + \frac{1}{D_n^h} [\bar{\Gamma}_n^h e^{-ik_{z_n}((z+z')-2z_{n+1})} + \bar{\Gamma}_n^h e^{-ik_{z_n}(2z_n-(z+z'))} \\ + \bar{\Gamma}_n^h \bar{\Gamma}_n^h e^{-ik_{z_n}(2(z_n-z_{n+1})-(z-z'))} + \bar{\Gamma}_n^h \bar{\Gamma}_n^h e^{-ik_{z_n}(2(z_n-z_{n+1})+(z-z'))}])]$$

Here z_n and z_{n+1} are the heights of the interface above and below layer n and D_n^h is defined as $D_n^h = [1 - \bar{\Gamma}_n^h \bar{\Gamma}_n^h e^{-ik_{z_n}2(z_n-z_{n+1})}]$. Note in particular that for layer zero where $\bar{\Gamma}_0^h = 0$ and $D_0^h = 1$ equation (9) reduces to,

$$(VIII-9b) \quad E_v^{J_v}(z | z'; k_{z_0}) = \frac{Z_0^h}{2} (e^{-ik_{z_0}|z-z'|} + \bar{\Gamma}_0^h e^{-ik_{z_0}((z+z')-2z_1)})$$

Identical results follow from equation (V-10) of section V,

$$(VIII-10) \quad E_u^{J_u}(z | z'; k_{z_n}) = \frac{Z_n^e}{2} (e^{-ik_{z_n}|z-z'|} + \frac{1}{D_n^e} [\bar{\Gamma}_n^e e^{-ik_{z_n}((z+z')-2z_{n+1})} + \bar{\Gamma}_n^e e^{-ik_{z_n}(2z_n-(z+z'))} \\ + \bar{\Gamma}_n^e \bar{\Gamma}_n^e e^{-ik_{z_n}(2(z_n-z_{n+1})-(z-z'))} + \bar{\Gamma}_n^e \bar{\Gamma}_n^e e^{-ik_{z_n}(2(z_n-z_{n+1})+(z-z'))}])]$$

Again noting that since for layer zero $\bar{\Gamma}_0^e = 0$, equation (10) reduces to,

$$(VIII-10b) \quad E_u^{J_u}(z | z'; k_{z_0}) = \frac{Z_0^e}{2} (e^{-ik_{z_0}|z-z'|} + \bar{\Gamma}_0^e e^{-ik_{z_0}((z+z')-2z_1)})$$

Equations (VIII-9b) and (VIII-10b) give the TE (E_v^J) and TM (E_u^J) components of the electric field Green functions for the Samtec Board. As was shown above in equations (VIII-3) and (VIII-4), repeated here, these electric field Green functions are then used to specify the components of the dyadic and scalar magnetic potential Green functions which are then used in the MoM process.

$$(VIII-3) G_{uu}^{AJ} = G_{vv}^{AJ} = \frac{1}{i\omega} E_v^J \quad (VIII-4) G_\phi = \frac{-i\omega}{k_u^2} (E_v^J - E_u^J)$$

Although we are able to calculate the complete magnetic potential dyadic Green function in each layer, the complete set of components will not be used (and hence not tested) during the validation process discussed below. It follows from the limitation remarks made previously, that equations (VIII-9b) and (VIII-10b) will be the only components required to analyze this structure.

Transforming from the spectral to the spatial domain

As discussed in section VII, $G_{uu}^{AJ}(z|z';k_{zn}) = E_v^J(z|z';k_{zn})/i\omega$ and the remaining component functions need to be inverse Fourier/Hankel transformed back to the spatial domain for use in the Method-Of-Moments procedure. To do this, the Green functions are first evaluated along a one-level approximation path. In GLMoM, the default one-level approximation path is specified by,

$$(VIII-11) k_z = k_0[.9(1-t) - i50t], \quad 0 \leq t \leq 1$$

This integration path is similar to the path described in section VII with $T_0 = 50$. Figure 8 shows the integration path as mapped to the $k_\rho = \sqrt{k_0^2 - k_z^2}$ plane. The Green functions are assumed to be negligible outside of this truncated path.

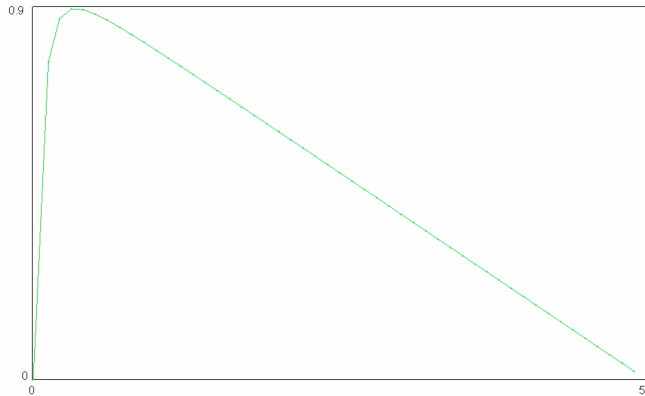


Figure 8. Integration path in the $k_\rho = \sqrt{k_0^2 - k_z^2}$ plane

As described in section VII, the functions $i2k_{zn}G$ (along the integration path) are approximated using the GPOF method,

$$i2k_{zn}G \approx \sum_{m=1}^N a_m e^{-b_m k_{zn}}$$

The accuracy of this approximation is strongly depended on the oscillatory and decay-rate behavior of the functions $i2k_z G$. As part of the verification process, spectral plots of these functions for the Samtec Reference structure will be examined to check for any such anomalies.

Figure 9 shows a magnitude plot of $G_\phi \cdot 2ik_z$ in the spectral domain along the contour given in Figure 8 at frequencies of 1GHz, 5 GHz, and 10 GHz (and $z = z' = 0$). From the figure we see that at 1 GHz the function converges very smoothly and moderately fast. At the higher frequencies of 5 GHz and 10 GHz a peak begins to become evident at values near $t = 0$ in the parameterization of equation (VIII-11). These values map to the far-field in the spatial domain [10].

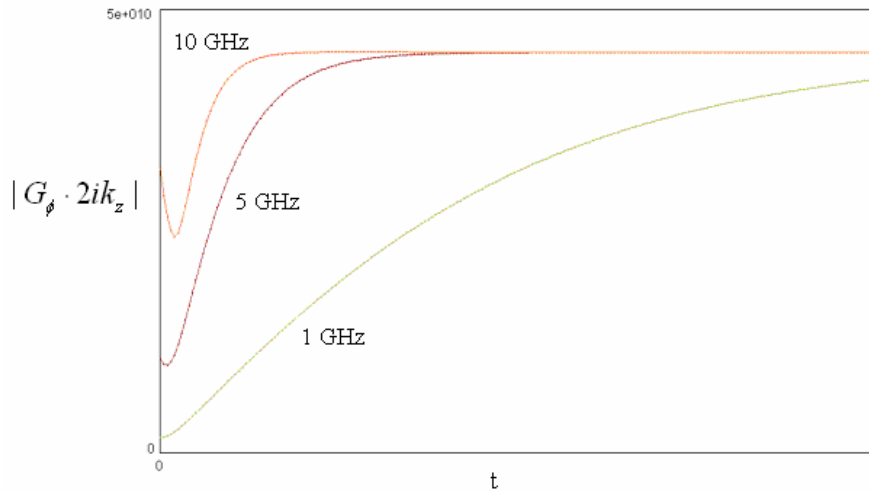


Figure 9. Spectral plot of $|G_\phi \cdot 2ik_z|$ at 1 GHz, 5 GHz, and 10 GHz

To validate the accuracy of the inverse Fourier/Hankel transformations performed by GLMoM (by way of exponential approximation) we compare them with a direct numerical integration. This comparative process can be conducted using a utility tool, MLGreen (also developed by Yaxun Liu). Figure 10 gives the results of this comparison where we have overlaid the plots given by numerical integration and exponential approximation. As expected there is some deviation in the far-field at higher frequencies (where the Green function is oscillatory in the spectral domain) but this deviation is less than 1% and so can be considered sufficiently accurate.

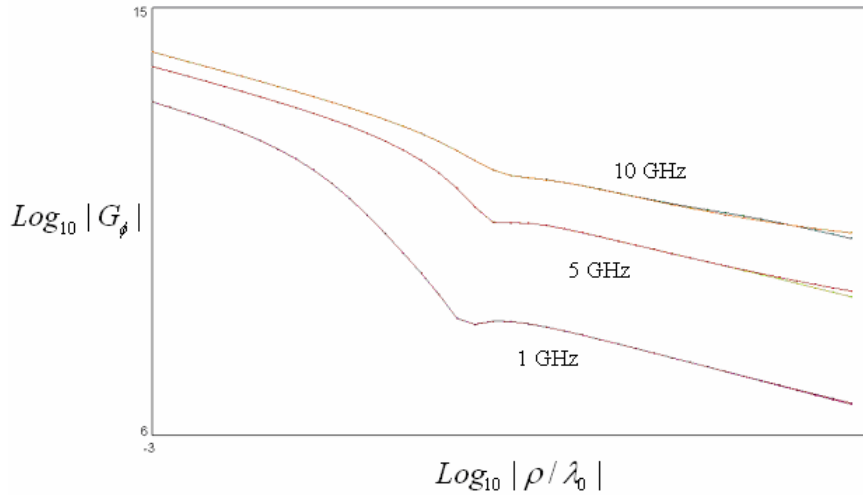


Figure 10. Spatial plot of $\text{Log}_{10} |G_\phi|$ at 1 GHz, 5 GHz, and 10 GHz

The validation process is then repeated for the G_{uu}^{AJ} component. Figure 11 shows a magnitude plot of $G_{uu}^{AJ} \cdot 2ik_z$ in the spectral domain along the contour given in Figure 8 at frequencies of 1GHz, 5 GHz, and 10 GHz (and $z = z' = 0$). Again from the figure we see that at 1 GHz the function converges very smoothly and moderately fast. At the higher frequencies of 5 GHz and 10 GHz a small peak begins to become evident.

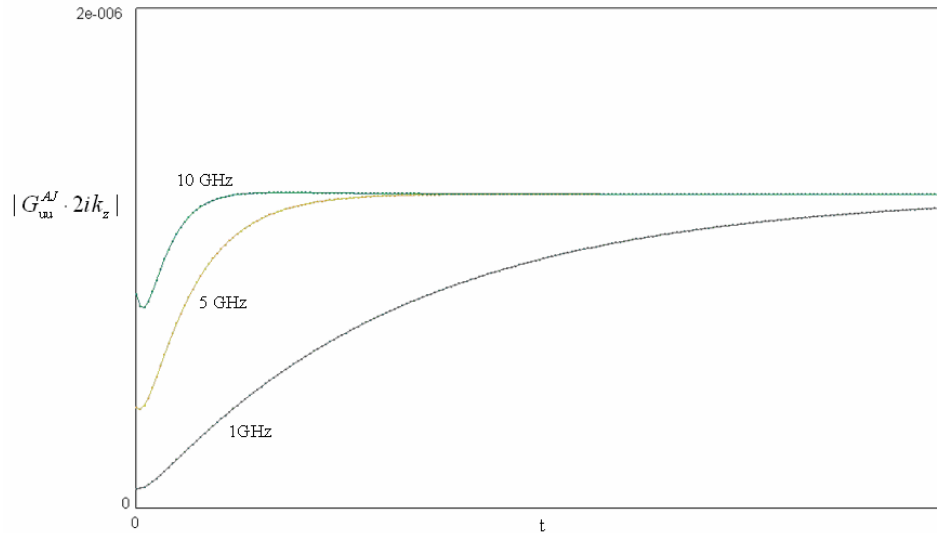


Figure 11. Spectral plot of $|G_{uu}^{AJ} \cdot 2ik_z|$ at 1GHz, 5 GHz, and 10 GHz

Figure 12 gives the results in the spatial domain where we have again overlaid the plots given by numerical integration and exponential approximation. The figure shows indiscernible differences between the two methods indicating excellent approximation.

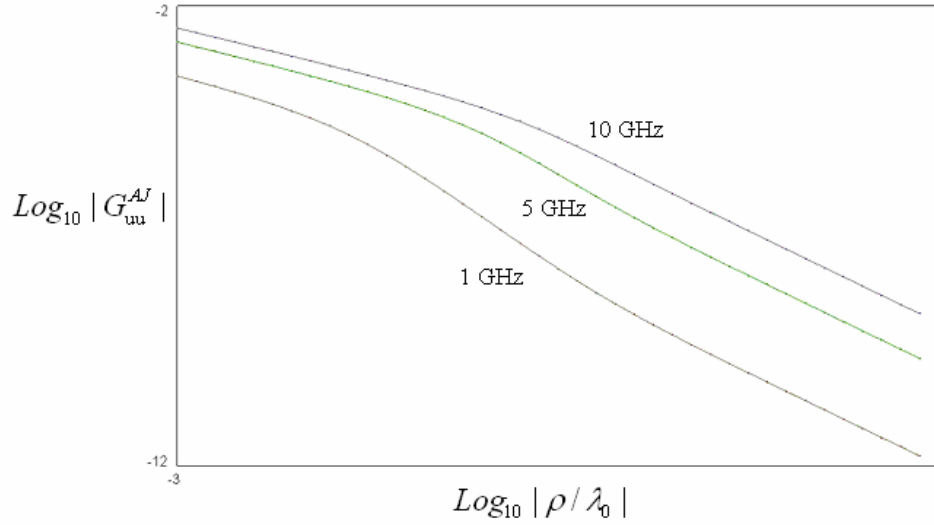


Figure 12. Spatial plot of $\text{Log}_{10} |G_{uu}^{AJ}|$ at 1 GHz, 5 GHz, and 10 GHz

We conclude from this analysis that the default one-level approximation gives sufficiently accurate results for inverse transforming the necessary Green functions from the spectral domain to the spatial domain. (We note that using GLMoM it is fairly straightforward to modify the integration path and/or change to higher level approximations were it found to be necessary.)

With the dyadic $\underline{\underline{\mathbf{G}}}^{AJ}$ and scalar G_ϕ Green functions validated for the given multi-layered structure, we now proceed with validating the use of these Green functions in the MoM integrals by finding the S-Parameters for the given metallization.

Measuring the Scattering Parameters

When entering the physical dimensions of the Samtec reference board into GLMoM (through the graphical OpenGL front end) additional feedline sections are added to ports 1 through 4 of Figure 5. A unit delta source is then numerically applied to the input of each port and the scattering parameters are calculated.

Figure 13 shows a schematic view of this process. Port 1 is shown driven with an input and the current distribution is then determined throughout the structure using the MoM procedure.



Figure 13. Determination of scattering parameters

The current on each of the feedlines (the Y sections in figure 13) is then approximated as a sum of forward and reverse traveling waves, as in,

$$I_n(x) = I_{n1}^+ e^{-i\beta_n x} + I_{n1}^- e^{+i\beta_n x}$$

where the subscripts refer to the amplitude on port n due to port 1 being excited. This process is then repeated for the remaining three ports and the scattering parameters determined from the matrix equation ref[15],

$$\begin{pmatrix} I_{11}^+ & I_{12}^+ & 0 & 0 \\ 0 & 0 & I_{11}^+ & I_{12}^+ \\ I_{21}^+ & I_{22}^+ & 0 & 0 \\ 0 & 0 & I_{21}^+ & I_{22}^+ \end{pmatrix} \begin{pmatrix} S_{11} \\ S_{12} \\ S_{21} \\ S_{22} \end{pmatrix} = \begin{pmatrix} -I_{11}^- \\ -I_{12}^- \\ -I_{21}^- \\ -I_{22}^- \end{pmatrix}$$

Terminology

Commonly used terms that are defined with respect to the calculated scattering parameters are [14]:

S_{11} - RL or Return Loss

S_{21} - IL or Insertion Loss

S_{31} - NEXT or Near-End Cross Talk

S_{41} - FEXT or Far-End Cross Talk

Crosstalk is often defined as the undesirable electromagnetic coupling between two or more conducting paths. NEXT is then defined as the unwanted signal coupling from a near-end transmitter into a pair of ports measured at the same end. FEXT is defined as the unwanted signal coupling from a transmitter at the near-end port into a pair of ports measured at the far-end [14].

Near-End Crosstalk (S31)

Samtec has performed extensive testing of the Golden Standard reference structure in both the frequency and time domain. A summary of the test results that includes information pertaining to the near-end (S31) and far-end (S41) cross talk is shown in table 1 and figure 14.

Software used	F_{S21min}	$F_{S31 \text{ 1st Peak}}$	Mag @ $F_{S31 \text{ 1st Peak}}$	F_{S41max}
PLTS (Full Board) Measured	7.34 GHz	320	-13.38	6.78 GHz
TDA (Full Board) Measured	7.36 GHz	320	-13.4	6.9 GHz

Table 1) Summary of Measured Data

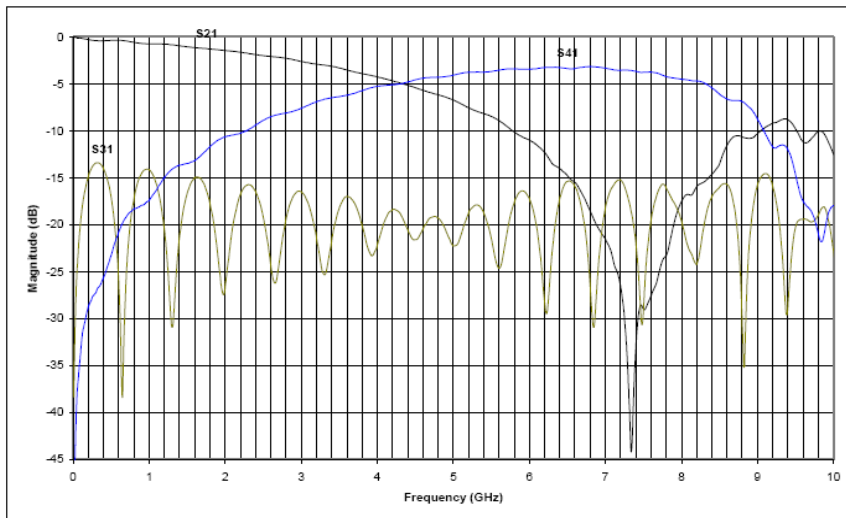


Figure 14. Plot of Measured Data

From Figure 14 (and table 1) it seen that the frequency of maximum coupling in S31 is 320 MHz (and $2n+1$ multiples). To test the low frequency capabilities of GLMoM we would like to verify its ability to locate these low frequency maxima. GLMoM implements the standard RWG basis so (as described in section II of this paper) we expect divergence below 500 MHz and therefore attempt to accurately locate the second maximum at 960 MHz. Figure 15 is a plot of a GLMoM simulation showing excellent agreement between simulated and measured values. Specifically it can be seen that the maximum S31 coupling of -14dB is accurately predicted at 960 MHz (.960 GHz) with less than 1% error.

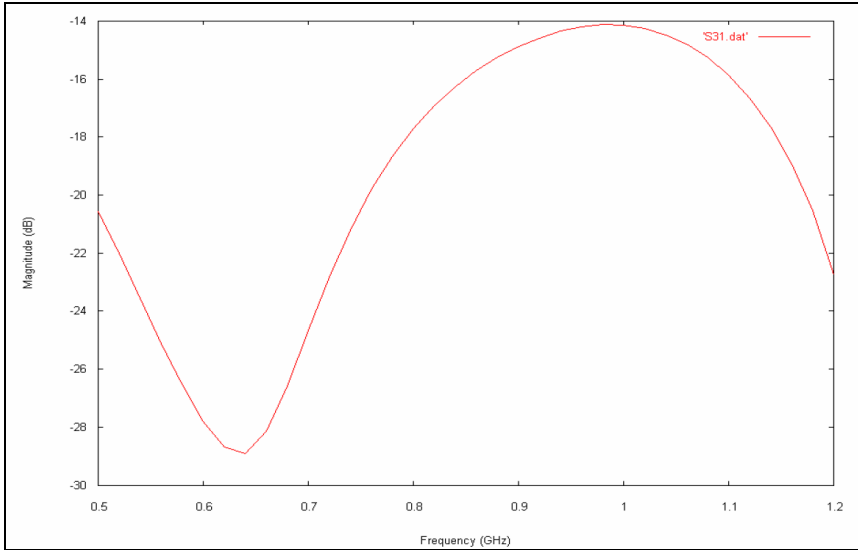


Figure 15. GLMoM Simulated Data

The mid to high frequency plot for the S31 parameter is shown in Figure 16. Again good agreement is shown between simulated and measured values.

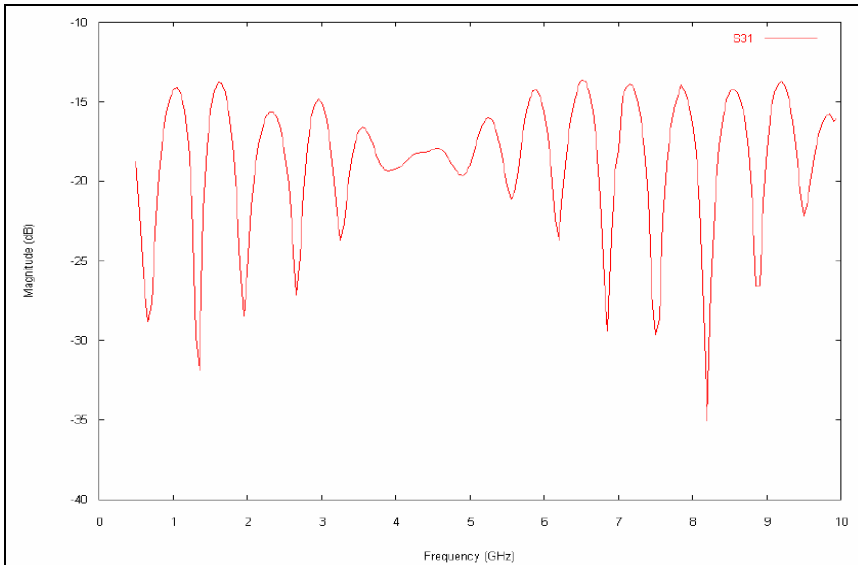


Figure 16. S13 GLMoM simulation

Far-End Crosstalk (S41)

The frequency for the maximum far-end crosstalk (S41) can be used as a high frequency marker for validation. The S41 maximum should occur slightly before the deep null of the S21 parameter due to broadband coupling [14]. Again comparing figures 14 and 17 shows good agreement between (GLMoM) simulated and (Samtec) measured data. Specifically it can be seen that the broadband coupling is accurately predicted by the relative positioning of the S41 maximum followed by the deep null in S21 around 7 GHz.

It should be noted that the specific frequency location of the S41/S21 maximum/null is highly dependent on permittivity.

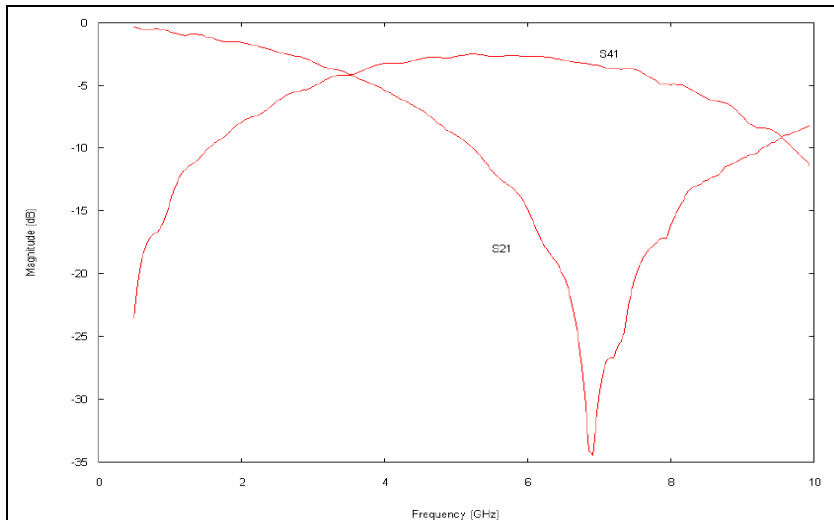


Figure 17. S41/S21 GLMoM simulation

Multiple simulations clearly show that lowering the permittivity results in raising the frequency of the S41/S21 maximum/null. With a relative permittivity $\epsilon_r = 1$, it was found that the S21 null occurs at approximately 13 GHz. This contradicts the statements made in ref [14] which attributes this frequency increase to the effects of added loss. Our simulations show that increasing dielectric loss (from a loss tangent of 0.02 to 0.08) merely decreases the magnitude of the S41/S21 parameters, by less than 3%, with virtually no effect on frequency dynamics.

Summary

A basic background of the theoretical aspects of Integral Equation Field Solvers was provided. The scalar and dyadic Green functions were derived and evaluated for the Samtec Golden Standard reference structure. These Green functions were then used in the Method-of-Moments process by GLMoM to calculate the surface currents over the conductors. S-Parameters were then discussed as a common specification for electromagnetic structures and a description then followed that expressed how field solvers determine these S-Parameters from the calculated current distribution. Finally, using the calculated S-Parameters of the Samtec reference structure, it was shown that GLMoM was capable of accurately predicting the near-end (S31) and far-end (S41) crosstalk over a large band-width.

If you have any questions or comments concerning this material, please feel free to contact Jim Rodgers at jrodger2@csulb.edu (www.csulb.edu/~jrodger2).

References

- [1] R Mavaddat, "Network scattering parameters"
- [2] D. Swanson, W. Hoefler, "Microwave circuit modeling using electromagnetic field simulation"
- [3] Weng Cho Chew, "Waves and fields in Inhomogeneous media"
- [4] Chen-To Tai, "Dyadic Green functions in electromagnetic theory"
- [5] Krzysztof A. Michalski and Dalian Zheng, "Electromagnetic scattering and radiation by surfaces of arbitrary shape"
- [6] Krzysztof A. Michalski and Juan R. Mosig, "Multilayered Media Green's Functions in Integral Equation Formulations".
- [7] M. Rao, D. Wilton, A. W. Gilsson, "Electromagnetic scattering by surfaces of arbitrary shape", IEEE. Trans. Vol.AP-30, NO.3, 1982, pp409-418
- [8] V. I. Okhmatovski, J. Morsey, and A.C. Cangellaris, "Loop-Tree Implementation of the Adaptive Integral Method (AIM) for Numerically Stable EM Modeling from Low to Multi-GHz Frequencies"
- [9] Ivar Stakgold, "Boundary value problems of mathematical physics"
- [10] M.I. Aksun, "A Robust Approach for the Derivation of Closed-Form Green's Functions".
- [11] Gulbin Dural, and M.I. Aksun, "Closed-Form Green's Functions for General Sources and Stratified Media".
- [12] Hua, Y., and T.K. Sakar, "Generalized pencil-of-functions method for extracting the poles of an electromagnetic system from its transient response".
- [13] Hua, Y., and T.K. Sakar, "Matrix pencil method for estimating parameters of exponentially damped/undamped sinusoids in noise".
- [14] Dan Piscotty, Julian Ferry, and Richard A. Elco, "The Samtec Golden Standard: A Reference Structure for Electrical Simulation and Measurement: Part 1 and Part 2".
- [15] Z. A. Maricevic and T.K. Sakar, "Analysis and measurements of arbitrarily shaped open microstrip structures".
- [16] Yaxun Liu, "GLMoM: An open-source EM simulator using Method of Moments".
- [17] J.D. Jackson, "Classical Electrodynamics, third edition".

Rev[1]

Appendix

In the cited literature (and software), network variables are defined as [6],

$$\bar{E}_t = E_u \hat{u} + E_v \hat{v} = V^e \hat{u} + V^h \hat{v}$$

$$\bar{H}_t = H_u \hat{u} + H_v \hat{v} = -I^h \hat{u} + I^e \hat{v} \quad \text{or} \quad \bar{H}_t \times \hat{z} = I^e \hat{u} + I^h \hat{v}$$

With sources

$$v^e = -M_v + \frac{k_\rho}{\omega \epsilon} J_z \quad \text{And} \quad i^e = -J_u$$

$$v^h = M_u \quad \text{And} \quad i^h = -\frac{k_\rho}{\omega \mu} M_z - J_v$$

Here J and M refer to the electric and magnetic current densities. Using these network variables, together with an $e^{-i\omega t}$ time dependence, allows the transmission line equations to be written in a form that is identical to the standard distributed parameter equations given in elementary transmission line theory. In this paper we have adopted the sign convention and terminology that is more common in electromagnetics [17].